# Electronic Structure and Properties of High-$T_c$ Superconducting Cuprates in the Normal and Superconducting Phases within the LDA + GTB Approach

**E. I. Shneyder[a, b], S. G. Ovchinnikov[a, c], M. M. Korshunov[a, c], and S. V. Nikolaev[c]**

[a] *Kirensky Institute of Physics, Siberian Branch, Russian Academy of Sciences, Akademgorodok, Krasnoyarsk, 660036 Russia*
*e-mail: shneyder@iph.krasn.ru*
[b] *Siberian State Aerospace University, Krasnoyarsk, 660014 Russia*
[c] *Siberian Federal University, Krasnoyarsk, 660041 Russia*
Received July 5, 2012

Theoretical investigations of the properties of high-$T_c$ superconducting cuprates within the LDA + GTB method taking into account the magnetic and phonon pairing mechanisms have been reviewed. These properties are the concentration-dependent electronic structure, quantum phase transitions with a change in the topology of the Fermi surface, and the superconducting phase of the $d_{x^2-y^2}$ symmetry.

## 1. INTRODUCTION

Although high-$T_c$ superconducting cuprates have long been studied, two global problems—(i) the nature of the "anomalous" normal state and (ii) mechanisms of superconductivity with the $d_{x^2-y^2}$ pairing symmetry—are still incompletely solved. What is the role of the electron (magnetic, charge, current) Bose-like fluctuations, along with phonons, in the formation of the superconducting state? How does a transition from a Mott–Hubbard insulator upon doping with holes or electrons to a Fermi liquid normal metal occur in highly doped cuprates through a non–Fermi liquid pseudogap state in the low-doping region? These and many other fundamental problems of the physics of high-$T_c$ superconductivity are currently the focus of attention. In our opinion, strong electron correlations in cuprates are responsible for such a slow progress in the theory of high-$T_c$ superconductivity. The traditional density functional theory methods are inapplicable in this situation. Several research groups are developing multielectron approaches to describe the electronic structure of systems with strong electron correlations (see [1]). In this review, we focus on the results obtained within the combined local density approximation (LDA) and generalized tight-binding (GTB) method. This combined method involves the ab initio LDA calculation of the parameters of the multielectron tight-binding Hamiltonian with the Coulomb interactions and cluster perturbation theory within the generalized tight-binding method [2, 3]. Within this approach, it is possible to construct a set of effective Hamiltonians with the form depending on the energy scale under consid-

eration. For example, to study the optical and photoelectron spectra on a scale of 10 eV, it is necessary to use the multiband $p–d$ model including various $d$ orbitals of copper and $p$ orbitals of oxygen [4]. To analyze angle-resolved photoemission spectroscopy (ARPES) data at a scale of 1−2 eV, it is possible to develop the two-band Hubbard model with singlet and triplet bands of Hubbard fermions; this model in the limit of strong correlations is modified to the singlet–triplet $t–J$ model [5]. Finally, to calculate the Fermi surface and superconducting pairing, it is sufficient to use the low-energy limit with one band of Hubbard fermions, which is described by the extended $t–J$ model, e.g., taking into account three-site correlated hopping (the $t–J^*$ model [6]) or four-spin ring exchange (the $t–J^*–J_c$ model [7]). In most cases, the parameters of these model Hamiltonians can be found from ab initio calculations, which are often nontrivial. In particular, the calculation of the effective exchange parameter between nearest neighbors in cuprates required the inclusion of all interband transitions within the multiband $p–d$ model; the signs of the exchange interaction involving singlet and triplet bands were antiferromagnetic and ferromagnetic, respectively [8]. The microscopic model Hamiltonians thus obtained are examined in various approximations from the mean field approximation for systems with strong electron correlations (Hubbard 1 approximation) to the generalized mean field approximation including the dependence of the static mass operator on the wave vector within cluster perturbation theory exactly taking into account the short-range order in 2 × 2 clusters. The results are usually in qualitative agreement with the experimental data and with

the calculations of other teams (Russian teams headed by A.F. Barabanov, V.V. Val'kov, and N.M. Plakida and many foreign teams; see references below). Below, we will consider the Fermi surfaces for various doping concentrations, compare the contributions from the magnetic and phonon pairing mechanisms, and describe changes in the electronic structure within the cluster approach.

## 2. ELECTRONIC STRUCTURE OF CUPRATES

Investigations of cuprates within the LDA + GTB method begin with the ab initio calculations of the electronic structure. Although the local density approximation does not provide the correct ground state of strongly correlated systems, the data thus obtained make it possible to determine, first, the minimum set of orbitals that should be included in the effective model and, second, the parameters of this model. To this end, the electronic structure of cuprates found in the LDA calculations is projected on Vanier functions in the basis of $p$ orbitals of oxygen and $e_g$ orbitals of copper [9]. It is noteworthy that the multiband $p-d$ model thus written includes the Coulomb interaction between electrons at one and several neighboring sites. Further, within the tight-binding method, the transition from the realistic multiband model to the effective low-energy singlet–triplet Hubbard model occurs in which the parameter $U_{eff} = E_{ct}$ describes the gap with charge transfer. In the limit of strong electron correlations, the model is simplified by the perturbation-theory exclusion of interband transitions and two-particle states of electrons [10, 11]. We note that we use the Hubbard operator representation in the effective Hamiltonian and in further calculations. This makes it possible to accurately take into account the constraint on the filling of two-particle states at one site. In this case, Hubbard operators are constructed on the eigenstates of the Hamiltonian of the $CuO_6$ cluster as $X_f^{pq} = |p\rangle\langle q|$ and describe hole quasiparticle excitations. The effective Hamiltonian of the upper Hubbard band of holes in single-layer cuprates has the form

$$H_{tJ^*} = H_{tJ} + H_{(3)}, \qquad (1)$$

$$H_{tJ} = \sum_{f,\sigma}(\varepsilon - \mu)X_f^{\sigma\sigma}$$

$$+ \sum_f (2\varepsilon - 2\mu + U_{eff})X_f^{22} + \sum_{f \neq g, \sigma} t_{fg} X_f^{2\sigma} X_g^{\bar\sigma 2}$$

$$+ \frac{1}{2}\sum_{f \neq g, \sigma} J_{fg}(X_f^{\sigma\bar\sigma}X_g^{\bar\sigma\sigma} - X_f^{\sigma\sigma}X_g^{\bar\sigma\bar\sigma}),$$

$$H_{(3)} = \sum_{f \neq m \neq g, \sigma} \frac{\tilde{t}_{fm}\tilde{t}_{mg}}{U_{eff}}(X_f^{2\bar\sigma} X_m^{\sigma\sigma} X_g^{\bar\sigma 2} - X_f^{2\sigma} X_m^{\sigma\bar\sigma} X_g^{\bar\sigma 2}).$$

Here, $\mu$ is the chemical potential of the system; $t_{fg}$ and $\tilde{t}_{fg}$ are the amplitudes of intra- and interband hops, respectively; $J_{fg} = t_{fg}^2/U_{eff}$ is the exchange interaction parameter; and $\bar\sigma \equiv -\sigma$. The following model parameters were obtained within the above scheme for the $La_2CuO_4$ compound: $t = 0.932$, $t' = -0.12$, $t'' = 0.152$, $J = 0.298$, $J' = 0.003$, and $J'' = 0.007$. The LDA + GTB scheme makes it possible to microscopically explain the necessity of the inclusion of intraband hops up to the third coordination sphere. Longer hops make only insignificant quantitative corrections to the dispersion of quasiparticles [9]. We also emphasize the role of three-site correlated hops $H_{(3)}$. These hops should be taken into account not only because the parameter $\tilde{t}_{fm}\tilde{t}_{mg}/U_{eff}$ and exchange integral $J_{fg}$ have the same order of magnitude. As was previously shown [6, 12], the three-site interactions strongly affect the spectrum of quasiparticle excitations in the presence of the short-range magnetic order in the system.

As is known, the inclusion of the interactions of an electron with the fluctuating short-range antiferromagnetic order provided agreement [13–16] between the quantum oscillation data [17, 18] and ARPES data [19, 20] at low doping. At the same time, the short-range antiferromagnetic order with the correlation length $\xi_{AFM} \approx 10$ Å also exists at optimal doping [21]. For this reason, it is topical to take into account this order not only in low-doped systems. At low temperatures ($T < 10$ K), fluctuations are quite slow with a characteristic lifetime of about $10^{-9}$ s at a scale of about the size of the antiferromagnetic microdomain $\xi_{AFM}$ [22]. This time is much larger than the characteristic times of the recovery of the equilibrium in the Fermi system in ARPES measurements ($10^{-13}$ s) [23] and the period of the rotation of the electron in a cyclotron orbit on the Fermi surface ($2\pi\omega_c^{-1} \approx 10^{-12}$ s, where $\omega_c$ is the cyclotron frequency) in the experiments reported in [17, 18]. Thus, when calculating the dynamics of the quasiparticle against the background of the antiferromagnetic order, the dynamics of the magnetic order itself can be neglected and only its spatial inhomogeneity should be taken into account. To calculate the corresponding corrections to the mass operator of the Green's function $G_{k\sigma}(E) = \langle\langle X_k^{\bar\sigma 2}|X_k^{2\bar\sigma}\rangle\rangle_E$, we used the method [24, 25] based on the projection of higher Green's functions on the function $G_{k\sigma}(E)$. Neglecting the dynamical corrections, we obtain [26, 12]

$$G_{k\sigma}(E) = \frac{(1+x)/2}{E - \varepsilon_0 + \mu - \frac{1+x}{2}t_k - \frac{1-x^2}{4}\frac{\tilde{t}_k^2}{U_{eff}} - \Sigma_k}, \quad (2)$$
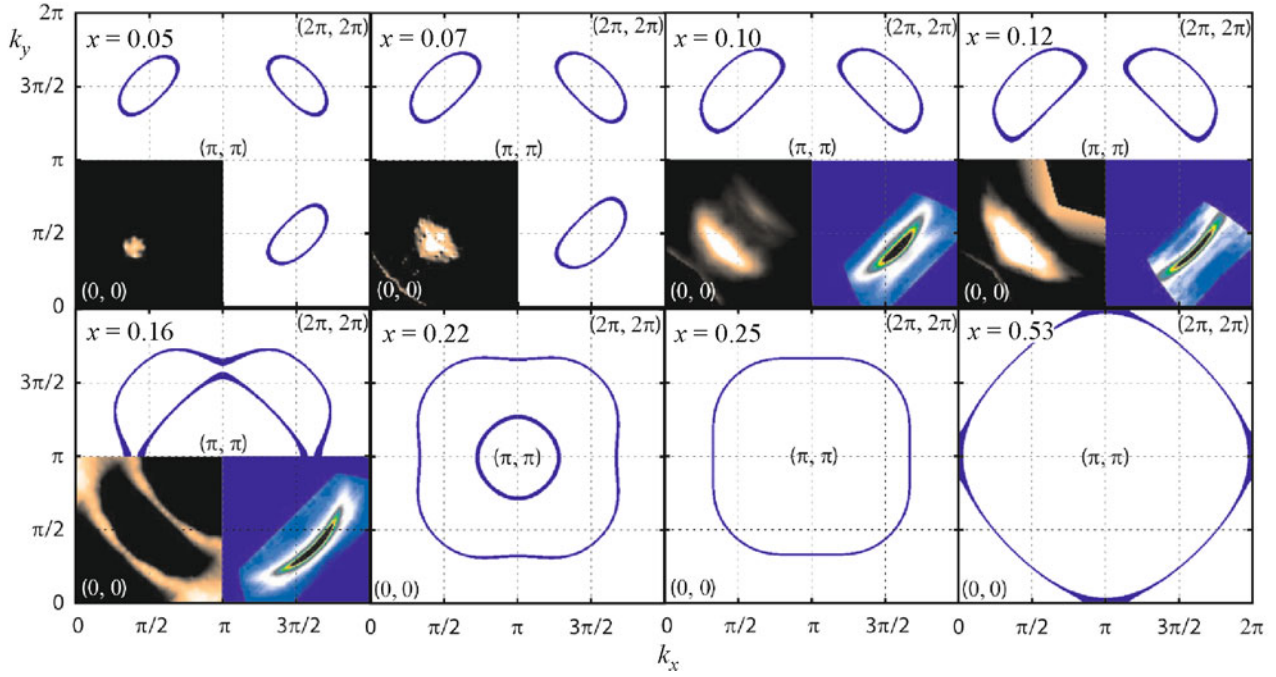
**Fig. 1.** Calculated sections of the Fermi surface in La$_{2-x}$Sr$_x$CuO$_4$ at various doping concentrations [27] in comparison with the ARPES data with different resolutions taken from (right corners) [28] and (left corners) [20]. The larger hole pocket becomes more circular with an increase in $x$.

where the mass operator $\Sigma_{\mathbf{k}}$ is expressed in terms of the static spin correlation function

$$C_{\mathbf{q}} = 2 \sum_{(\mathbf{f}-\mathbf{g})} e^{-i(\mathbf{f}-\mathbf{g})\mathbf{q}} \langle S_{\mathbf{f}}^z S_{\mathbf{g}}^z \rangle$$

and the kinematic spin correlation function

$$K_{\mathbf{q}} = 2 \sum_{(\mathbf{f}-\mathbf{g})} e^{-i(\mathbf{f}-\mathbf{g})\mathbf{q}} \langle X_{\mathbf{f}}^{2\bar{\sigma}} X_{\mathbf{g}}^{\bar{\sigma}2} \rangle$$

as

$$\Sigma_{\mathbf{k}} = \frac{2}{1+x}\frac{1}{N}$$

$$\times \sum_{\mathbf{q}} \left\{ \left[ t_{\mathbf{k}-\mathbf{q}} - \frac{1-x}{2}\left(J_{\mathbf{q}} - \frac{\tilde{t}_{\mathbf{k}-\mathbf{q}}^2}{U_{\mathrm{eff}}}\right) - \frac{(1+x)\tilde{t}_{\mathbf{k}}\tilde{t}_{\mathbf{k}-\mathbf{q}}}{U_{\mathrm{eff}}} \right] \right.$$

$$\left. \times \frac{3}{2}C_{\mathbf{q}} - \left[ t_{\mathbf{q}} - \frac{1-x}{2}J_{\mathbf{k}-\mathbf{q}} - x\frac{\tilde{t}_{\mathbf{q}}^2}{U_{\mathrm{eff}}} - \frac{(1+x)\tilde{t}_{\mathbf{k}}\tilde{t}_{\mathbf{q}}}{U_{\mathrm{eff}}} \right] K_{\mathbf{q}} \right\}.$$

The self-consistent calculation of the correlation functions $C_{\mathbf{q}}$ and $K_{\mathbf{q}}$ and chemical potential $\mu$ makes it possible to construct the family of Fermi surfaces for various doping concentrations (Fig. 1). The Fermi surface twice changes its topology with doping. At low doping, when the short-range magnetic order occurs, there are four hole pockets near the $(\pi/2, \pi/2)$ points, as could be expected for a hole in the antiferromagnetic phase. The size of hole pockets increases with doping. Near the first critical point $x_{c1} \approx 0.15$, a bridge is formed on the line $(\pi, 0)-(\pi, \pi)$. In the range between the first and second critical concentrations, $x_{c1} < x < x_{c2} \approx 0.24$, there are two surfaces centered at
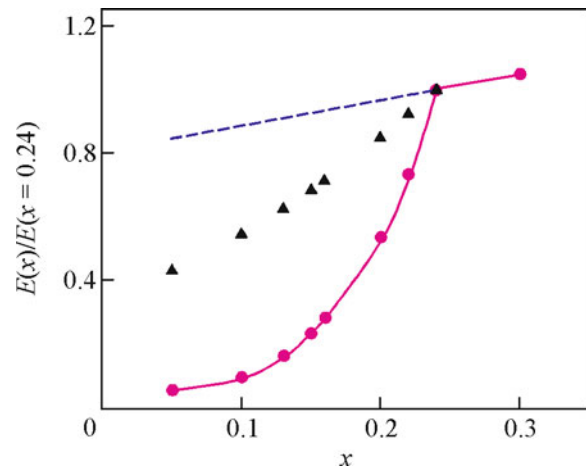
the point $(\pi, \pi)$. The smaller pocket is of electron character and disappears at $x \longrightarrow x_{c2}$. The large hole pocket becomes more circular with an increase in $x$. Only this pocket remains at $x > x_{c2}$. It is worth noting that the critical concentrations are calculated with a certain error. First, the model parameters were obtained through the complex procedure of the projection of the LDA wavefunctions on the Vanier function basis and can be changed when varying this basis. Second, the method for determining the Green's functions is approximate. The inclusion of higher order contributions can change quantitative values of the critical points. We believe that the qualitative picture at low temperature hardly changes, because it is determined by the general properties of the dispersion of the electron against the background of the fluctuating short-range antiferromagnetic order [27]. We also note that similar changes in the Fermi surface were obtained for the Hubbard model taking into account not only the real part of the mass operator but also its imaginary part [29], as well as in the calculations within the spin-fermion model [30]. A similar transformation with the appearance of a doubly connected Fermi surface in the intermediate composition range was recently revealed in the ab initio quantum-chemical calculations taking into account various multielectron configurations [31]. Qualitative agreement of our results with the mentioned calculations performed in various approximations is due to the common idea that the electronic structure is everywhere determined by the short-range magnetic order.
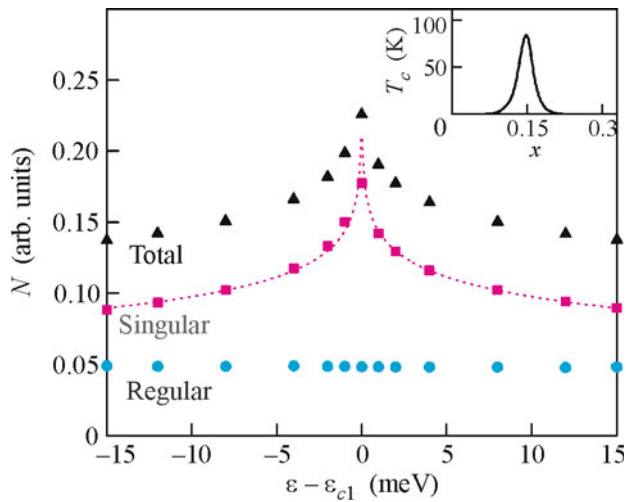
**Fig. 2.** Density of states calculated for the critical concentration $x_{c1} = 0.15$ as the sum of the regular and singular contributions, $\varepsilon_{c1} = \varepsilon_F(x_{c1})$ [34]. The dotted line corresponds to the logarithmic approximation for the singular contribution. The inset shows the concentration dependence of the superconducting transition temperature for $x_{opt} = x_{c1}$.



**Fig. 3.** Concentration dependence of the kinetic energy of holes [34]. The dashed line shows the usual behavior characteristic of a normal two-dimensional metal, triangles show the calculation in the idealized pseudogap model [38, 40], and circles show the calculation with Green's function (2).

Thus, the reported investigations of the doping-induced evolution of the Fermi surface of cuprates demonstrate a soft behavior of quasiparticle bands, which is common for all strongly correlated systems. According to [32, 33], transformations of the topology of the Fermi surface in a three-dimensional compound, which are due both to the appearance of a new segment and to a change in connectivity, are accompanied by the appearance of a singularity in the density of states, $\delta N(\varepsilon) \propto (\varepsilon - \varepsilon_c)^{1/2}$, and by a change in the thermodynamic potential $\delta\Omega \sim (\varepsilon_F - \varepsilon_c)^{5/2}$. In other words, quantum phase transitions in three-dimensional systems are 2.5-order transitions. Here, $\varepsilon_c$ is the energy of the quasiparticles at the critical point and $\varepsilon_F$ is the Fermi energy. We now consider singularities in the density of states of cuprates at the first and second critical points. We take into account that these compounds cannot be treated as isotropic three-dimensional systems because of strong anisotropy of the electronic and magnetic properties. Owing to this circumstance, calculations for single-layer cuprates can be performed only inside one $CuO_2$ plane.

The calculations show that the first critical point $x_{c1}$ corresponds to a logarithmic feature in the density of states. The disappearance of the electron pocket near the second critical point $x_{c2}$ is described by a Heaviside step feature [34]. We emphasize that both types of singularities are in agreement with the general properties of Van Hove singularities for two-dimensional electron systems [35]. In contrast to the universal behavior in three-dimensional systems, the thermodynamic potential of two-dimensional electrons has the addi-

tional singular contribution $\delta\Omega \sim (\varepsilon_F - \varepsilon_c)^2$ in the case of the step singularity in the density of states or the additional singular contribution $\delta\Omega \sim (\varepsilon_F - \varepsilon_c)^2 \ln|\varepsilon_F - \varepsilon_c|$ in the case of the logarithmic singularity [36]. Thus, the quantum phase transition in cuprates at $x_{c2}$ is a second-order transition. The singularity at the first critical point $x_{c1}$ is stronger. Therefore, the Sommerfeld parameter $\gamma = C_e/T$ determined by the electron specific heat also has a step singular term at $x \approx 0.24$ and has a logarithmic jump $\delta\gamma \propto \ln(\varepsilon_F - \varepsilon_c) \propto \ln(x - x_{opt})$ at $x \approx 0.15$. A similar jump of the specific heat was revealed within the Hubbard model by the continuous-time dynamical cluster quantum Monte Carlo method [37].

The fact that the doping-induced evolution of the properties of cuprates from the Mott−Hubbard insulator to a normal metal is not smooth and passes through a number of quantum critical points is widely discussed. Some authors [38−42] attribute the critical concentration to the formation of a pseudogap state at $x < p^*$, where $p^* = 0.19-0.24$. At the same time, according to the Hall effect measurements [43, 44], the quantum phase transition occurs at the optimal doping $p_{opt} = 0.15$. The calculations of the concentration dependences of the superconducting transition temperature $T_c(x)$ and the kinetic energy of holes $E_{kin}(x)$ performed within the proposed approach show that the coincidences between $x_{c1}$ and $p_{opt}$, as well as between $x_{c2}$ and $p^*$, are not accidental (Figs. 2, 3). First, the maximum of the critical temperature in the BCS theory is determined by the maximum in the density of states. For this reason, considering the exchange mechanism of superconducting pairing in

model (1), we conclude [45] that the optimal doping indeed corresponds to the critical concentration: $x_{opt} = 0.15 = x_{c1}$ (Fig. 2). Second, an analysis indicates that the kinetic energy of charge carriers $E_{kin}(x) = \sum_n t_{0n} K_{0n}(x)$ decreases strongly at $x < 0.24$ (Fig. 3). This decrease in the kinetic energy is described by an exponential law $E_{kin}(x)/E_{kin}(x_{c2}) = \exp[-4\Delta_{pg}/J]$ with the pseudogap parameter $\Delta_{pg}$ depending on the doping concentration. For the doping concentrations above the critical value $x > 0.24$, the behavior of the function $E_{kin}$ is usual, characteristic of a normal two-dimensional metal with the concentration of holes $n_h = 1 + x$; i.e., the kinetic energy is proportional to the Fermi energy and number of holes, $E_{kin} \sim \xi_F \sim n_h$. We attribute a decrease in the kinetic energy at concentrations $x < x_{c2}$ to the formation of the pseudogap, which is qualitatively confirmed by the calculations of $E_{kin}(x)$ in the simplest model [38, 40] of the electron gas with a triangular pseudogap.

Similar sequences of doping-induced transformations of the Fermi surface were obtained within the $p-d$ model in [29], where the dynamical corrections of the mass operator of the Green's function were taken into account in the disjoint diagrams approximation, and in [46, 47] for a Mott−Hubbard insulator in the cluster generalization of the dynamical mean field theory. In spite of differences in details (both poles and zeros of the Green's function were revealed in [46, 47]), similar evolutions of the electronic structure in our approach and in works where dynamical correlations were taken into account indicate that the proposed method is applicable, at least for low temperatures. In this limit, the properties of the normal phase of strongly correlated systems are significantly determined by the spatial inhomogeneity of correlations. The character of the $k$ dependence of the self-energy part of the Green's function plays a significant role in the description of electron correlations in CuO planes [48, 49] and the phase diagram of cuprates [50, 51]. A further development of the proposed method undoubtedly requires the inclusion of dynamical effects. Below, we describe one of the variants for such a development.

## 3. PROBLEMS OF THE DESCRIPTION OF SUPERCONDUCTING STATE IN SYSTEMS WITH STRONG ELECTRON CORRELATIONS

Any commonly accepted concept of the mechanism of the formation of a superconducting state in cuprates is still absent. The problem is that such a concept should explain not only high transition temperatures, but a whole set of unusual properties of these compounds. At the same time, the appearance of kinks in the dispersion law observed by the ARPES methods [19], excitations in the spectra obtained with inelastic neutron and X-ray scattering [52−54], and features of

tunnel experiments [55, 56] can be interpreted in alternative scenarios of pairing owing to the interaction of electrons both with spin excitations and with phonons. The phonon and electron contributions to the function $\Pi(\Omega)$ describing the interaction of fermion quasiparticles with boson excitations were separated in [57] using nonequilibrium optical spectroscopy with femtosecond resolution. The calculation of the corresponding coupling constants showed that the phonon contribution is smaller than the electron one by a factor of only two and cannot be neglected. In the absence of a clearly dominant pairing mechanism, the superconducting state of cuprates should be described within a self-consistent theory including the interactions of electrons with various boson excitations, both electron and phonon. The characteristic times of these interactions are different. For this reason, the dynamical retardation effects (see, e.g., [58]) should be taken into account in the complete realistic picture. This problem is generally very difficult. It begins with the mean field theory formulated for the strong electron correlation regime. Below, we briefly report some results obtained in model (1) including the electron−phonon interaction.

One of the key problems of the physics of high-$T_c$ superconductors is the study of the temperature isotopic effect, i.e., a strongly nonmonotonic doping dependence of the isotopic effect exponent $\alpha(x)$ [59]. The exponent $\alpha(x)$ is minimal at the optimal doping point and is almost an order of magnitude smaller than a value of 1/2 predicted in the BCS theory for normal metals and reaches its maxima at the boundaries of the superconducting state. The isotopic effect exponent in a low doped sample is much larger than 1/2. Some authors treated this behavior as evidence of a smallness of the electron−phonon contribution to the pairing potential. However, considering the BCS theory superconductivity taking into account competing exchange and phonon pairing mechanisms, we showed that the form of the concentration dependence of the isotopic effect constant, i.e., the positions of the minimum and maxima of the function $\alpha(x)$, is determined by the logarithmic singularity in the density of states near the critical point $x_{c1} = x_{opt}$. In this case, it does not correlate with the relation between the pairing coupling constants [60], whose doping dependence has strong singularities [61]. We do not discuss the asymmetric growth of the isotopic effect exponent near the boundaries of the superconductivity region. First, our approach begins with the atomic limit and, for this reason, overestimates the contribution to the self-energy in the band limit, i.e., for a highly doped sample. Second, we disregard the possible admixture to the superconducting OP from the $d_{x^2-y^2}$ component with the $s$ symmetry in the low-doping region [62−64], where real compounds undergo a transition from the tetragonal phase to the orthorhombic one. Furthermore, we ignore the charge-ordering
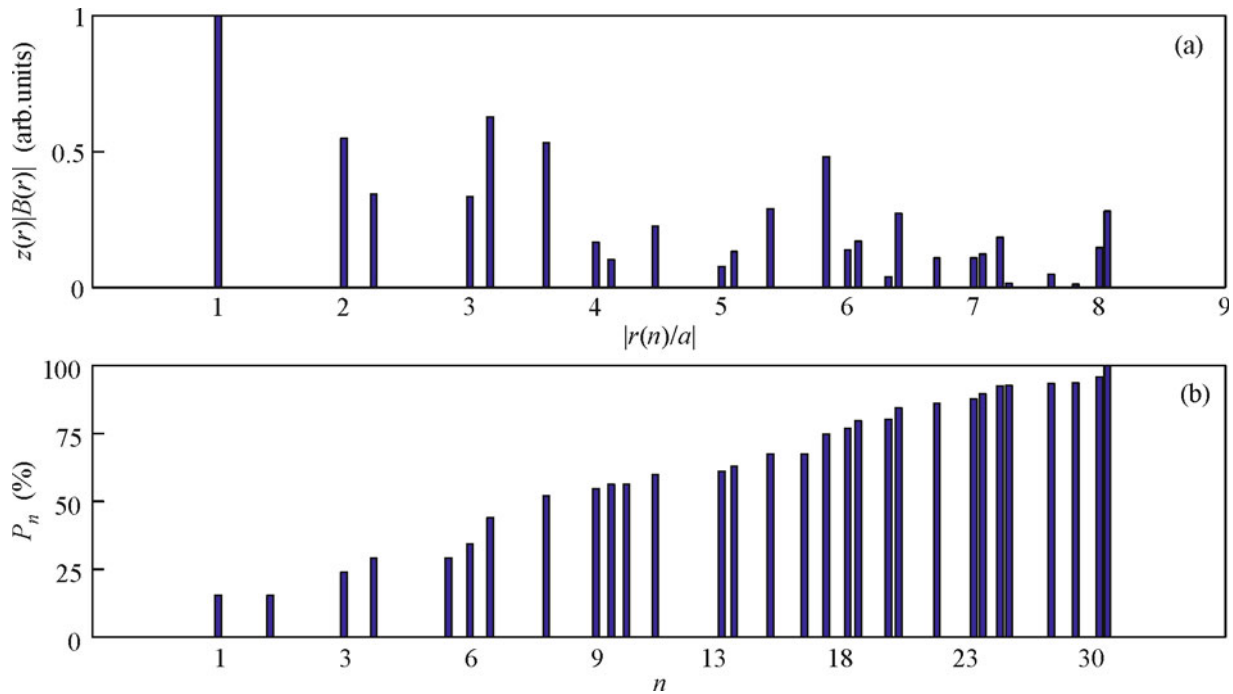
**Fig. 4.** (a) Correlation function and (b) fraction of correlations taken into account for the $n$th coordination sphere [66].

effects responsible for the anomalies in the properties of the $La_{2-x}Sr_xCuO_4$ at $x = 1/8$.

Below, we discuss the description of superconductivity in systems with strong electron correlations within numerical nonperturbative cluster approaches. The calculated pair correlation functions are usually very small. For this reason, various authors made different conclusions about the possibility of $d_{x^2-y^2}$ superconductivity in the strong correlation regimes within the Hubbard model or $t–J$ model (see discussion in [65]). At the same time, in all numerical methods such as the quantum Monte Carlo method and exact diagonalization of the cluster, investigations of magnetic pairing mechanisms are limited by a finite size of the cluster. For this reason, the reliability of the results obtained taking into account pairing only at the nearest neighbors is an open question. We considered the correlation function $B_{\mathbf{q}} = \langle X_{\mathbf{q}}^{\sigma 2} X_{-\mathbf{q}}^{\bar{\sigma} 2} \rangle$ describing superconducting pairing of Hubbard fermions in the $t–J$ model for the BCS theory [66]. Correlations are nonlocal, are spatially distributed, and decrease slowly with the distance. The size obtained for a Cooper pair is close to the experimental value $\xi \approx 30$ Å of the correlation length in high-$T_c$ superconductors. For a two-dimensional square lattice, we also analyzed the product of the correlation function $|B(\mathbf{r})|$ and the number of neighbors $z_n$ in the $n$th coordination sphere (Fig. 4a) and, correspondingly, the fraction of correlations $P_n$ that are taken into account when only the $n$th coordination sphere is included (Fig. 4b). According to the

calculations, the contribution of the first coordination sphere is not determining and is no more than 20% of the total value. These results indicate that the numerical calculations for small clusters strongly underestimate the energy gain in the superconducting phase as compared to the normal phase.

To conclude this section, we give an example demonstrating the competition between various exchange pairing mechanisms in cuprates. As is known, a number of properties experimentally observed in cuprates cannot be explained within the usual Heisenberg Hamiltonian. The observed anomalous structure of spectra of spin excitations can be described only by taking into account four-spin ring exchange processes [67–71]. According to the cited works, the magnitude of the ring exchange $J_c$ in the $CuO_2$ plane is smaller than the Heisenberg exchange $J$ only by a factor of 3–5. For this reason, there is a question: How significant is its effect on the Cooper pairing owing to magnetic interactions? We showed [7] that the equation for the superconducting transition temperature in the BCS theory for Hamiltonian (1) taking into account the ring exchange can be represented in the form similar to the equation for $T_c$ in the $t–J$ model:

$$1 = \tilde{J} \frac{1}{N} \sum_{\mathbf{p}} \frac{(\cos p_x - \cos p_y)^2}{\xi_{\mathbf{p}}} \tanh \frac{\xi_{\mathbf{p}}}{2k_B T_c}. \qquad (3)$$

Here, $\xi_{\mathbf{p}}$ is the dispersion of quasiparticles in the superconducting phase and $k_B$ is the Boltzmann constant. We separate the contributions of the Heisenberg

exchange, three-site hopping, and ring exchange in the renormalized coupling constant:

$$\tilde{J} = \left(1 - \frac{1+x}{2} + C_{01}\frac{J_c}{J}\right)J.$$

The ring exchange, as well as three-site correlated hopping [6], suppresses superconducting pairing induced by the Heisenberg exchange. This is obvious because the antiferromagnetic spin correlator $C_{01}$ for nearest neighbors is negative. Although the contribution from the ring exchange to the coupling constant is much smaller than the Heisenberg contribution, its relative role increases in the consistent development of the theory taking into account three-site hopping, which reduces the critical temperature by an order of magnitude. For the characteristic parameters of the LSCO system [9], the critical temperature in the $t$–$J^*$–$J_c$ model is 25–30% smaller than that in the $t$–$J^*$ model. We recall that the intersite Coulomb interaction weakly screened in cuprates [72, 73] is another mechanism compensating the Heisenberg exchange contribution to Cooper pairing. This demonstrates the problem of the relation between various mechanisms of superconducting pairing in real compounds.

## 4. CLUSTER PERTURBATION THEORY IN THE REPRESENTATION OF HUBBARD OPERATORS

The above results were obtained in the generalized Hartree–Fock approximation. As was mentioned above, its main disadvantage is the absence of correlations. One of the possible variants for the development of the theory involves the cluster perturbation theory [74, 75], which has long been proposed to study the high-$T_c$ superconducting cuprates [76–78]. The application of the cluster approach to study systems with strong electron correlations expands [49] owing to the main advantage of this method—direct inclusion of strong electron correlations and short-range order, which is significant for the description of low-dimensional magnetic systems.

A feature of the proposed approach is the use of the representation of the Hubbard $X$ operators. This makes it possible to simplify the implementation of the method and, more important, to introduce a quantity controlling the calculation error, which significantly reduces the computation time [79]. At the first stage, the exact diagonalization of the cluster (structure element of the superlattice), which is determined by the possibility of covering the initial lattice, is performed. Then, the intercluster interaction is taken into account within perturbation theory. The Hamiltonian of the two-dimensional single-band Hubbard model has the form

$$H = \sum_{i\sigma}\left[(\varepsilon - \mu)n_{i\sigma} + \frac{U}{2}n_{i\sigma}n_{i\bar{\sigma}}\right] - \sum_{i \neq j, \sigma} t_{ij}a_{i\sigma}^{\dagger}a_{j\sigma}. \quad (4)$$

Here, $a_{i\sigma}^{\dagger}$ and $a_{i\sigma}$ are the creation and annihilation operators for an electron with spin $\sigma$ at the $i$th site, $n_{i\sigma} = a_{i\sigma}^{\dagger}a_{i\sigma}$ is the operator of the number of electrons with spin $\sigma$ ($\bar{\sigma} = -\sigma$), $\varepsilon$ is the energy of the electron on the site, $\mu$ is the chemical potential, $t_{ij}$ is the hopping integral from the $j$th site to the $i$th site, and $U$ is the Coulomb interaction parameter at the site. Equation (4) is written for a square lattice whose structure parameter is one site. Another structure element can be defined in the same lattice. We take it in the form of a $2 \times 2$ square cluster. Thus, we can describe the initial lattice in terms of a new lattice with a basis (superlattice). We group the terms in Hamiltonian (4) so as to separate the intracluster interactions from intercluster interactions:

$$H = \sum_{f}H_0^c(f) + \sum_{f \neq g}H_1^c(f, g), \quad (5)$$

where $f$ and $g$ are cluster indices. In the description of the electronic structure by Hamiltonian (4), the Hubbard $X$ operators are defined at single-site eigenstates. Generalizing this procedure, we define the $X$ operators at cluster eigenstates. To this end, we obtain the complete set of eigenstates and eigenvectors of the Hamiltonian $H_0^c(f)$ by the exact diagonalization method. As a result, we obtain the following expansion for the annihilation operator of an electron at the $i$th site belonging to the $f$th cluster in the cluster $X$ operators:

$$a_{fi\sigma} = \sum_{\alpha}\gamma_{i\sigma}(\alpha)X_f^{\alpha}, \quad \gamma_{i\sigma}(\alpha) = \langle n|a_{i\sigma}|m\rangle. \quad (6)$$

Here, $X_f^{\alpha} \equiv |n\rangle\langle m|$, where $\alpha = \alpha(n, m)$; $n$ and $m$ mark the initial and final states of the cluster, respectively; and $f$ is the cluster index. The properties of $X$ operators were described in detail in [80–83]. According to Eq. (6), the electron can be represented in the form of the superposition of certain quasiparticles, Hubbard fermions $X_f^{\alpha}$; each quasiparticle corresponds to excitation from multiparticle initial state $|m\rangle$ to multiparticle final state $|n\rangle$. This procedure was described in more detail in [79].

Using expansion (6), Hamiltonian (4) can be represented in the form

$$H = \sum_{fn}\varepsilon_n X_f^{nn} + \sum_{f \neq g}\sum_{\alpha\beta}t_{fg}^{\alpha\beta}X_f^{\dagger\alpha}X_g^{\beta}, \quad (7)$$

where $\varepsilon_n$ is the energy of the cluster in the $n$th state and $t_{fg}^{\alpha\beta}$ are the intercluster hopping integrals. To obtain the dependence on the wave vector, it is necessary to transfer from the direct space to the reciprocal one. Below, we will be interested only in intercluster interaction in Hamiltonian (7). Taking into account the

uniformity of the lattice, this interaction can be represented as

$$H_1 = \sum_{\mathbf{k}} \sum_{\alpha\beta} T_{\alpha\beta}(\tilde{\mathbf{k}}) X_{\mathbf{k}}^{\dagger\alpha} X_{\mathbf{k}}^{\beta}, \tag{8}$$

where $\tilde{\mathbf{k}}$ is the wave vector in the reduced Brillouin zone. The procedure of the formation of the cluster lattice was described in detail in [84].

We seek the Green's function $D_{\alpha\beta}(\tilde{\mathbf{k}}, \omega) = \langle\langle X_{\tilde{\mathbf{k}}}^{\alpha} | X_{\tilde{\mathbf{k}}}^{\dagger\beta} \rangle\rangle_{\omega}$ in the Hubbard-I approximation. The matrix equation for the Green's function has the form

$$D^{-1}(\tilde{\mathbf{k}}, \omega) = [D^0(\omega)]^{-1} - T(\tilde{\mathbf{k}}), \tag{9}$$

where

$$D_{\alpha\beta}^0(\omega) = \frac{F(\alpha)}{\omega - \Omega(\alpha)}\delta_{\alpha\beta}, \tag{10}$$

$$\Omega(\alpha) = \varepsilon_m(N+1) - \varepsilon_n(N) - \mu, \tag{11}$$

$$F(\alpha) \equiv F(n, m) = \langle X^{nn} \rangle + \langle X^{mm} \rangle. \tag{12}$$

Here, $D^0(\omega)$ is the local (i.e., cluster) Green's function, $F(\alpha)$ is the filling factor, $\mu$ is the chemical potential, and $N$ is the number of electrons in the cluster. To analyze the electronic properties, it is necessary to calculate the single-particle Green's function, $G_{\sigma}(\mathbf{k}, \omega) = \langle\langle a_{\mathbf{k}\sigma} | a_{\mathbf{k}\sigma}^{\dagger} \rangle\rangle_{\omega}$, defined on the initial lattice. In terms of the Green's function in the $X$ representation defined on the superlattice, the single-particle Green's function can be determined from Eq. (9) without breaking the translational symmetry as [75, 79]

$$G_{\sigma}(\mathbf{k}, \omega) = \frac{1}{N_c} \sum_{\alpha, \beta}^{N_c} \sum_{i, j = 1} \gamma_{i\sigma}(\alpha)\gamma_{j\sigma}^*(\beta) \\ \times D_{\alpha\beta}(\mathbf{k}, \omega)e^{-i\mathbf{k}(\mathbf{r}_i - \mathbf{r}_j)}, \tag{13}$$

where $N_c$ is the number of sites in the cluster (in our case, $N_c = 4$), $k$ is the wave vector defined in the initial Brillouin zone, and $i$ and $j$ are the indices of the intracluster sites. Here, we took into account that the Green's function $D_{\alpha\beta}(\tilde{\mathbf{k}}, \omega)$ is a periodic function in the reciprocal space of the superlattice and the wave vector $\mathbf{k}$ can be represented in the form $\mathbf{k} = \mathbf{K} + \tilde{\mathbf{k}}$, where $\mathbf{K}$ is the translation vector of the reciprocal superlattice. Therefore, $D_{\alpha\beta}(\tilde{\mathbf{k}}, \omega) = D_{\alpha\beta}(\mathbf{k}, \omega)$ [49]. The Green's function $G_{\sigma}(\mathbf{k}, \omega)$ and corresponding spectral function

$$A_{\sigma}(\mathbf{k}, \omega) = -\frac{1}{\pi}\lim_{\delta \to +0}[\text{Im}G_{\sigma}(\mathbf{k}, \omega + i\delta + \mu)] \tag{14}$$

are calculated in the initial Brillouin zone.

When all possible excitations are taken into account in the representation of $X$ operators (6), the following sum rule is satisfied:

$$\langle[a_{i\sigma}, a_{i\sigma}^{\dagger}]_+\rangle = \sum_{\alpha} |\gamma_{i\sigma}(\alpha)|^2 F(\alpha) = 1. \tag{15}$$

As was mentioned above, the total spectral weight of the Fermi quasiparticles is controlled in all our calculations by the $f$ factor introduced in [79] as

$$\int d\omega A_{\sigma}(\mathbf{k}, \omega) = \sum_{\alpha} |\gamma_{i\sigma}(\alpha)|^2 F(\alpha) \equiv f. \tag{16}$$

In the case of the exact calculation, $f = 1$. All results presented below were obtained with $f > 0.995$. It appeared that the number of energy levels under consideration can be strongly reduced so that the error in the sum rule is no more than one percent. For this reason, we call our version of cluster perturbation theory as norm conserving cluster perturbation theory.

We consider the doping procedure in the described calculation scheme [84]. We define the doping concentration $x$ as the concentration of holes in the cluster. The exact diagonalization of the Hamiltonian of the $2 \times 2$ cluster provides the complete set of eigenvalues and eigenvectors which specify the Hilbert space. At half filling and $T = 0$, the transitions between the ground state in the subspace with $N = 4$ and states in subspaces with $N = 3$ and $N = 5$ have nonzero filling factor (12). In the case of hole doping, it is necessary to take into account the possibility of population of the ground state in the subspace with $N = 3$. As a result, additional transitions with a nonzero filling factor appear. We consider only single-electron transitions with a change in the number of particles by 1. Since the number of sites in the cluster is 4, doping per cluster $x$ is expressed in terms of doping per site $p$ as $x = 4p$.

The main results obtained within the norm conserving cluster perturbation theory are as follows. The calculated energy of the ground state as a function of $U$ [84] is in good agreement with the results obtained by nonperturbative variation and quantum Monte Carlo methods [85, 86]. Agreement with the exact diagonalization calculations for the $4 \times 4$ cluster is very good [87]. Comparison with [88], where variational cluster perturbation theory was used, shows good agreement at small $U$ values and provides the best result at larger $U$ values.

The "rigid band" representation is inapplicable to study systems with strong electron correlations. It is known that doping of such systems leads to the formation of in-gap states [89], which appear in the band gap and can significantly change the conducting properties of these systems. Our cluster calculations taking into account hops between the nearest neighbors show the presence of such in-gap states [84]. The distribution of the spectral weight over the Hubbard bands and intraband states has an interesting feature. The num-
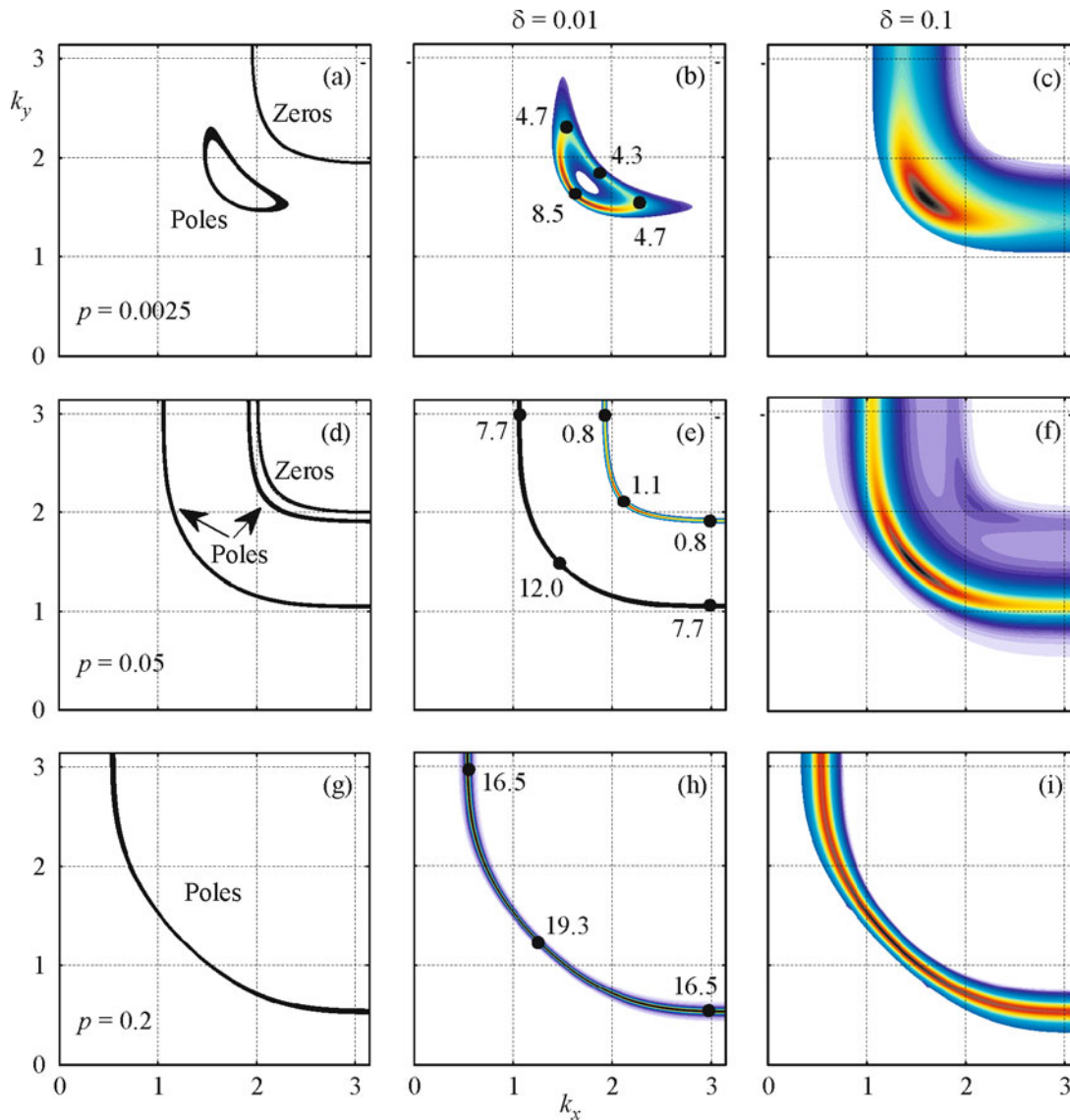
**Fig. 5.** Concentration dependences of the (a, d, g) Fermi surface and maps of the spectral weight at broadening $\delta$ = (b, e, h) 0.01$t$ and (c, f, i) 0.1$t$. The numbers on panels (b, e, h) show the inhomogeneous distribution of the spectral weight [91].

ber of states in the lower Hubbard band at $U = 12t$ is insufficient for all electrons of the system. For this reason, some electrons occupy in-gap states. According to the calculation, the number of in-gap states is sufficient for these electrons. Thus, the Fermi level in the low-doping region and at $U = 12t$ is in the band of in-gap states, where its pinning occurs [90, 84].

To compare the results with the situation in real cuprates, we took into account the effect of hopping between non-nearest sites [84]. In the case of the $2 \times 2$ cluster, hopping between the first and second neighbors is already taken into account in the calculation of the eigenstates of the cluster. Hopping between third neighbors is taken into account only in the intercluster interaction. The calculations with the parameters from [12] showed the presence of pseudogap states and

an inhomogeneous distribution of the spectral weight of quasiparticles over the Fermi surface [91]. Analysis of a series of quantum phase transitions with doping demonstrated that such changes in the electronic structure can be observed in experiments only with the corresponding high resolution. In our calculations, the energy resolution is determined by the half-width of the Lorentzian $\delta$.

It is noteworthy that the Green's function has not only poles but also zeros. This was shown within the cluster dynamic mean field theory in [46, 92]. The structure of poles and zeros obtained in our calculation (Figs. 5a, 5d, 5g) qualitatively coincides with the results obtained in [92]. The sequence of topological transformations of the Fermi surface corresponds to the results obtained in [12, 30, 27]. The distribution of
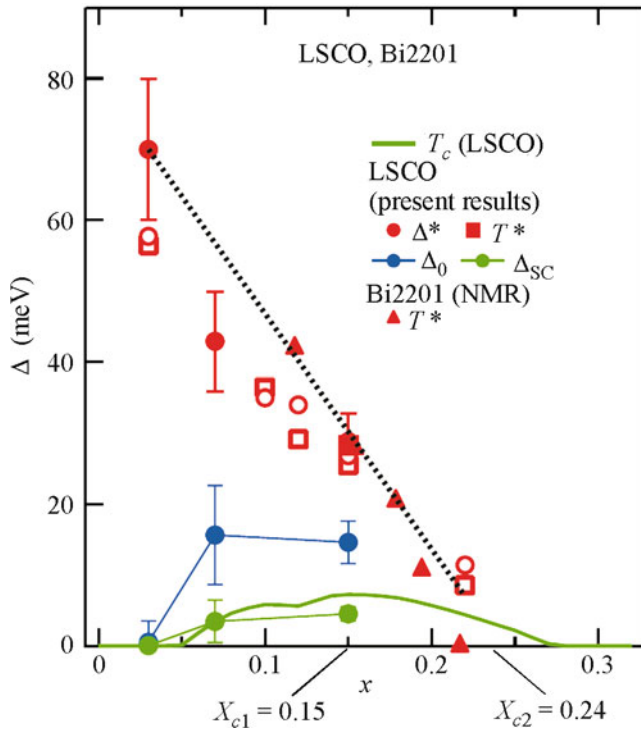
**Fig. 6.** Experimental phase diagram of single-layer cuprates [93] and the calculated quantum critical points [27].

the spectral weight $A(\mathbf{k}, \varepsilon_F)$ in the limit $\delta \longrightarrow 0$ should provide the same picture of the Fermi surface that is obtained from the analysis of dispersion laws. Indeed, the comparison of the first and second columns in Fig. 5 provides a similar picture. The maps of the spectral weight show its inhomogeneous distribution in the Brillouin zone. Similar regions with a low spectral weight were previously obtained in [30]. However, the third column ($\delta = 0.1$), rather than second column ($\delta = 0.01$), in Fig. 5 corresponds to the really observed ARPES spectra. The broadening of lines corresponding to $\delta = 0.1$ is large so that the small pocket is closed to an arc (Fig. 5c), whereas only one arc instead of two concentric pockets around the $(\pi, \pi)$ point is observed in the intermediate concentration region (Fig. 5f). The ARPES picture corresponds to the actual Fermi surface only in the high concentration region, where there is one large surface (Figs. 5g, 5h, 5i). It is worth noting that, despite a qualitative similarity of the evolution of the Fermi surface with doping described in the preceding section [12], the critical concentrations of Lifshitz transitions do not coincide. These values depend on the model (spin-fermion model [30], Hubbard model [29], or $t$–$J$ model [12]), on the parameters of the model, and on the approximation under consideration.

Small hole pockets in low doped cuprates were experimentally revealed when measuring Landau quantum oscillations in high magnetic fields [17]. The

smearing of pockets to arcs upon broadening was established by many authors [46, 13]. We showed that broadening leads to the smoothing of the picture of Lifshitz transitions and to a smooth healing of the pseudogap near the $(\pi, 0)$ antinodal point. The length of the arc measured in ARPES is small in the doping region $p \leq 0.05$ and increases gradually with $p$. The constancy of the spectral weight along the Fermi surface at $p \geq 0.25$ corresponds to the expected Fermi liquid behavior.

According to the results reported above, the distribution of the spectral intensity over the Brillouin zone observed in ARPES at the linewidth $\delta = 0.1t$ cannot provide the actual topology of the Fermi surface in high-$T_c$ superconducting cuprates. Only a decrease in the linewidth by an order of magnitude makes it possible to obtain the actual Fermi surface from the spectral intensity distribution.

Thus, the cluster approach even in the Hubbard-I approximation for the intercluster interactions reproduces the main features of systems with strong electron correlations. This is primarily due to the exact inclusion of the short-range order in the system. The difference of our cluster perturbation theory from similar theories is the use of the $X$ Hubbard operator technique. This made it possible to introduce the $f$ factor to control the total spectral weight of quasiparticles in the necessary accuracy limits [79, 84].

## 5. CONCLUSIONS

In this short publication, we have focused on our methods and results and have not discussed many other theories. We only mentioned that other approaches to the description of superconductivity in cuprates and the Hubbard model include the cluster methods (VCA [94], CDMFT [95, 96], DCA [97, 98], see also review [49]), functional renormalization group [99, 100], quantum Monte Carlo method [101], bipolaron theories [102], theory of magnetic three-spin polarons [103] (which is a new interesting variant of multielectron theory), spin-fluctuation theories (FLEX [104, 105] and others [58, 106]), theory of resonance valence bonds [107], and Gutzwiller approximation [108].

It is commonly accepted that the physics of the high-$T_c$ superconducting cuprates is determined by two characteristic energy scales—superconducting gap and pseudogap [93]. We have demonstrated within the proposed approach that the evolution of the electronic structure of cuprates at low temperatures passes through two quantum critical points (Fig. 6). One of them, optimal doping point $x_{c1}$, is associated with the formation of the maximum in the $T_c(x)$ dependence. The other point, $x_{c2}$, lies at the interface of the transition from the Fermi liquid state to non-Fermi liquid one and coincides with the linear extrapolation of the concentration dependence of the temperature of the formation of the pseudogap state $T^*(x)$ to the intersection with the

abscissa axis (Fig. 6). The first critical point coincides with the experimental value $x_{opt}$ in Fig. 6.

## REFERENCES

1. *Theoretical Methods for Strongly Correlated Systems*, Ed. by A. Avella and F. Mancini, Springer Series in Solid-State Sciences, Vol. 171 (Springer, Berlin, 2012), p. 505.

2. M. M. Korshunov, V. A. Gavrichkov, S. G. Ovchinnikov, et al., J. Exp. Theor. Phys. **126**, 642 (2004).

3. S. G. Ovchinnikov, V. A. Gavrichkov, M. M. Korshunov, and E. I. Shneyder, in *Theoretical Methods for Strongly Correlated Systems*, Ed. by A. Avella and F. Mancini, Springer Series in Solid-State Sciences, Vol. 171 (Springer, Berlin, 2012), p. 143; W. F. Brinkman and M. C. Cross, in *Progress in Temperature Physics*, Ed. by D. F. Brewer (North Holland, Amsterdam, 1978), Vol. 7A, p. 105.

4. V. A. Gavrichkov, S. G. Ovchinnikov, A. A. Borisov, et al., J. Exp. Theor. Phys. **91**, 369 (2000).

5. M. M. Korshunov and S. G. Ovchinnikov, Phys. Solid State **43**, 416 (2001).

6. V. V. Val'kov, T. A. Val'kova, D. M. Dzebisashvili, et al., JETP Lett. **75**, 378 (2002).

7. E. I. Shneyder, S. G. Ovchinnikov, and A. Shnurenko, JETP Lett. **95**, 193 (2012).

8. V. A. Gavrichkov and S. G. Ovchinnikov, Phys. Solid State **50**, 1081 (2008).

9. M. M. Korshunov, V. A. Gavrichkov, S. G. Ovchinnikov, et al., Phys. Rev. B **72**, 165104 (2005).

10. L. Bulaevskii, E. Nagaev, and D. Khomskii, Sov. Phys. JETP **27**, 836 (1968).

11. K. A. Chao, J. Spalek, and A. M. Oles, J. Phys. C **10**, L271 (1977).

12. M. M. Korshunov and S. G. Ovchinnikov, Eur. Phys. J. B **57**, 271 (2007).

13. E. Z. Kuchinskii, I. A. Nekrasov, and M. V. Sadovskii, JETP Lett. **82**, 198 (2005).

14. E. Z. Kuchinskii and M. V. Sadovskii, J. Exp. Theor. Phys. **103**, 415 (2006).

15. N. Harrison, R. D. McDonald, and J. Singleton, Phys. Rev. Lett. **99**, 206406 (2007).

16. E. Z. Kuchinskii and M. V. Sadovskii, JETP Lett. **88**, 192 (2008).

17. N. Doiron-Leyrand, C. Proust, D. LeBoeuf, et al., Nature **447**, 565 (2007).

18. E. A. Yelland, J. Singleton, C. H. Mielke, et al., Phys. Rev. Lett. **100**, 047003 (2008).

19. A. Damacelli, Z. Hussein, and Z. X. Shen, Rev. Mod. Phys. **75**, 473 (2003).

20. J. Meng, G. Liu, W. Zhang, et al., Nature **462**, 335 (2009).

21. T. R. Thurston, R. J. Birgeneau, M. A. Kastner, et al., Phys. Rev. B **40**, 4585 (1989).

22. S. M. Haden, G. Aeppli, H. Mook, et al., Phys. Rev. Lett. **66**, 821 (1991).

23. D. Mihailovic and V. V. Kabanov, Supercon. Complex Syst. **114**, 331 (2005).

24. N. M. Plakida, V. Yu. Yushankhay, and I. V. Stasyuk, Physica C **162–164**, 787 (1989).

25. V. Yu. Yushankhay, N. M. Plakida, and P. Kalinay, Physica C **174**, 401 (1991).

26. V. V. Val'kov and D. M. Dzebisashvili, J. Exp. Theor. Phys. **100**, 608 (2005).

27. E. I. Shneyder and S. G. Ovchinnikov, J. Exp. Theor. Phys. **109**, 1017 (2009).

28. M. Hashimoto, T. Yoshida, H. Yagi, et al., Phys. Rev. B **77**, 094516 (2008).

29. N. M. Plakida and V. S. Oudovenko, J. Exp. Theor. Phys. **104**, 230 (2007).

30. A. F. Barabanov, A. A. Kovalev, O. V. Urazaev, et al., J. Exp. Theor. Phys. **92**, 677 (2001).

31. L. Hozoi, M. S. Laad, and P. Fulde, Phys. Rev. B **78**, 165107 (2008).

32. I. M. Lifshits, Sov. Phys. JETP **11**, 1130 (1960).

33. I. M. Lifshits, M. Ya. Azbel', and M. I. Kaganov, *Electron Theory of Metals* (Nauka, Moscow, 1971; Consultants Bureau, Adam Hilger, New York, 1973).

34. S. G. Ovchinnikov, E. I. Shneyder, and M. M. Korshunov, J. Condens. Matter **23**, 045701 (2011).

35. J. M. Ziman, *Principles of the Theory of Solids* (Cambridge Univ. Press, Cambridge, 1964).

36. S. S. Nedorezov, Sov. Phys. JETP **24**, 578 (1966).

37. K. Mikelsons, K. Khatami, E. Galanakis, et al., Phys. Rev. B **80**, 140505(R) (2009).

38. J. R. Cooper and J. W. Loram, J. Phys. IV France **10**, Pr3-213 (2000).

39. J. W. Loram, J. Luo, J. R. Cooper, et al., J. Phys. Chem. Solids **62**, 59 (2001).

40. J. L. Tallon, J. W. Loram, G. V. M. Williams, et al., Phys. Status Solidi B **215**, 531 (1999).

41. C. Castellani, C. Di Castro, and M. Grilli, Z. Phys. B **103**, 137 (1997).

42. R. Daou, N. Doiron-Leyraud, D. LeBoeuf, et al., Nature Phys. **5**, 31 (2009).

43. F. F. Balakirev, J. B. Betts, A. Migliori, et al., Nature **424**, 912 (2003).

44. F. F. Balakirev, J. B. Betts, A. Migliori, et al., Phys. Rev. Lett. **102**, 017004 (2009).

45. E. I. Shneyder and S. G. Ovchinnikov, JETP Lett. **83**, 394 (2006).

46. S. Sakai, Y. Motome, and M. Imada, Phys. Rev. Lett. **102**, 056404 (2009).

47. S. Sakai, Y. Motome, and M. Imada, Phys. Rev. B **82**, 134505 (2009).

48. M. H. Hettler, A. N.-Z. Tahvildar, T. Pruschke, et al., Phys. Rev. B **58**, R7475 (1998).

49. T. Maier, M. Jarrell, T. Pruschke, et al., Rev. Mod. Phys. **77**, 1027 (2005).

50. K. Haule and G. Kotliar, Phys. Rev. B **76**, 104509 (2007).

51. B. Kyung, D. Séńechal, and A.-M. S. Tremblay, Phys. Rev. B **80**, 205109 (2009).

52. T. Dahm, V. Hinkov, S. V. Borisenko, et al., Nature Phys. **5**, 217 (2009).

53. D. Reznik, L. Pintschovius, M. Ito, et al., Nature **440**, 1170 (2006).

54. M. Le Tacon, G. Ghiringhelli, J. Chaloupka, et al., Nature Phys. **7**, 725 (2011).

55. J. Lee, K. Fujita, K. McElroy, et al., Nature **442**, 546 (2006).

56. O. Ahmadi, L. Coffey, J. F. Zasadzinski, et al., Phys. Rev. Lett. **106**, 167005 (2011).

57. S. Dal Conte, C. Giannetti, G. Coslovich, et al., Science **335**, 1600 (2012).

58. N. M. Plakida and V. S. Oudovenko, Phys. Rev. B **59**, 11949 (1999).

59. M. K. Crawford, W. E. Farneth, E. M. McCarronn, et al., Science **250**, 1390 (1990).

60. E. I. Shneyder and S. G. Ovchinnikov, J. Exp. Theor. Phys. **109**, 1017 (2009).

61. E. I. Shneyder and S. G. Ovchinnikov, JETP Lett. **83**, 394 (2006).

62. A. G. Sun, D. A. Gajewski, M. B. Maple, et al., Phys. Rev. Lett. **72**, 2267 (1994).

63. R. Kleiner, A. S. Katz, A. G. Sun, et al., Phys. Rev. Lett. **76**, 2161 (1996).

64. Q. Li, Y. N. Tsay, M. Suenaga, et al., Phys. Rev. Lett. **83**, 4160 (1999).

65. T. Aimi and M. Imada, J. Phys. Soc. Jpn. **76**, 084709 (2007).

66. S. G. Ovchinnikov and E. I. Shneyder, Phys. Solid State **53**, 242 (2011).

67. S. Sugai, M. Sato, T. Kobayashi, et al., Phys. Rev. B **42**, 1045 (1990).

68. J. Lorenzana, J. Eroles, and S. Sorella, Phys. Rev. Lett. **83**, 5122 (1999).

69. R. Coldea, S. M. Hayden, G. Aeppli, et al., Phys. Rev. Lett. **86**, 5377 (2001).

70. A. A. Katanin and A. P. Kampf, Phys. Rev. B **66**, 100403 (2002).

71. M. Roger and J. M. Delrieu, Phys. Rev. B **39**, 2299 (1989).

72. A. S. Alexandrov and V. V. Kabanov, Phys. Rev. Lett. **106**, 136403 (2011).

73. N. M. Plakida, arXiv: 1110.6715v1.

74. A.-M. S. Tremblay, B. Kyung, and D. Séńechal, Low Temp. Phys. **32**, 424 (2006).

75. D. Séńechal, D. Perez, and D. Plouffe, Phys. Rev. B **66**, 075129 (2002).

76. A. F. Barabanov, L. A. Maksimov, and A. V. Mikheenkov, Sov. Phys. Solid State **30**, 1449 (1988).

77. A. F. Barabanov, L. A. Maksimov, and A. V. Mikheyenkov, J. Phys.: Condens. Matter **1**, 10143 (1989).

78. S. G. Ovchinnikov and I. S. Sandalov, Physica C **161**, 607 (1989).

79. S. V. Nikolaev and S. G. Ovchinnikov, J. Exp. Theor. Phys. **111**, 635 (2010).

80. J. Hubbard, J. Proc. R. Soc. A **285**, 542 (1965).

81. V. V. Val'kov and S. G. Ovchinnikov, *Quasiparticles Strongly Correlated Systems* (Sib. Otd. Ross. Akad. Nauk, Novosibirsk, 2001) [in Russian].

82. R. O. Zaitsev, Sov. Phys. JETP **41**, 100 (1975).

83. R. O. Zaitsev, *Diagrammatic Methods in Theory of Superconductivity and Ferromagnetism* (URSS, Moscow, 2004) [in Russian].

84. S. V. Nikolaev and S. G. Ovchinnikov, J. Exp. Theor. Phys. **114**, 118 (2012).

85. H. Yokoyama and H. Shiba, J. Phys. Soc. Jpn. **56**, 3582 (1987).

86. J. E. Hirsch, Phys. Rev. B **31**, 4403 (1985).

87. G. Fano, F. Ortolani, and A. Parola, Phys. Rev. B **42**, 6877 (1990).

88. C. Dahnken, M. Aichhorn, W. Hanke, et al., Phys. Rev. B **70**, 245110 (2004).

89. S. G. Ovchinnikov, Sov. Phys. JETP **75**, 283 (1992).

90. S. V. Nikolaev and S. G. Ovchinnikov, Zh. SFU, Matem. Fiz. **4**, 162 (2011).

91. S. G. Ovchinnikov and S. V. Nikolaev, JETP Lett. **93**, 517 (2011).

92. T. D. Stanescu and G. Kotliar, Phys. Rev. B **74**, 125110 (2006).

93. T. Yoshida, M. Hashimoto, S. Ideta, et al., Phys. Rev. Lett. **103**, 037004 (2009).

94. M. Aichhorn, E. Arrigoni, M. Potthoff, et al., Phys. Rev. B **74**, 024508 (2006).

95. A. I. Lichtenstein and M. I. Katsnelson, Phys. Rev. B **62**, R9283 (2000).

96. M. Capone and G. Kotliar, Phys. Rev. B **74**, 054513 (2006).

97. T. Maier, M. Jarrell, T. Pruschke, et al., Phys. Rev. Lett. **85**, 1524 (2000).

98. R. Arita and K. Held, Phys. Rev. B **73**, 064515 (2006).

99. C. J. Halboth and W. Metzner, Phys. Rev. B **61**, 7364 (2000).

100. C. Honerkamp and M. Salmhofer, Phys. Rev. B **64**, 184516 (2001).

101. S. Sorella, G. B. Martins, F. Becca, et al., Phys. Rev. Lett. **88**, 117002 (2002).

102. A. S. Alexandrov, Phys. Rev. B **61**, 12315 (2000).

103. V. V. Val'kov, D. M. Dzebisashvili, and A. F. Barabanov, JETP Lett. **92**, 618 (2010).

104. N. E. Bickers, D. J. Scalapino, and S. R. White, Phys. Rev. Lett. **62**, 961 (1989).

105. T. Dahm and L. Tewordt, Phys. Rev. Lett. **74**, 793 (1995).

106. T. A. Maier, D. Poilblanc, and D. J. Scalapino, Phys. Rev. Lett. **100**, 237001 (2008).

107. P. W. Anderson, Science **235**, 1196 (1987).

108. D. Baeriswy, D. Eichenberger, and B. Gut, Phys. Status Solidi B **244**, 2299 (2007).

*Translated by R. Tyapaev*